

Analytical and Experimental Study of Squirrel Cage Induction Motors with rotor bars faults

A. Ghoggal, M. Sahraoui, S. E. Zouzou

LGEB Laboratory, University of Mohamed khider, BP. 145, 07000, Biskra, Algeria

Abstract

In this paper, we present an analytical approach in order to study in efficiency way the spectral contents of the stator line currents of three-phase squirrel cage induction motors with broken rotor bars. This study is based on analytical expressions for the stator and the cage rotor magneto motive forces (MMF) which are derived using the winding function approach. Also, a simple approach is used to study the influence of broken rotor bars on the rotor cage MMF in order to estimate the frequencies of the spectral components induced in the stator windings. This approach assumes that one broken bar means that one rotor loop is absent. Consequently, the new rotor cage MMF, with broken bar, can be obtained by subtracting rotor MMF induced by the absent loop from the healthy rotor MMF. In addition, and taking into account the time supply harmonics, general expressions independent from the number of pole pairs are established which give frequencies of all related spectral components. This approach and the theoretical predictions are verified tanks to appropriate experimental tests.

Keywords

Diagnosis, induction motors, fault detection, winding function, stator current monitoring.

1. Introduction

Three-phase squirrel cage induction motors are the most common prime machines in industrial processes. This is chiefly due to their low coast, reasonable size, ruggedness and low maintenance. In industrialized nations, they can typically consume between 40 to 50% of all the generated capacity of these countries (Thomson-a 2001). Usually, the induction motors work under many stresses from various nature (thermal, electric, mechanical and environment) which can affect their lifespan by involving the occurrence of stator and/or rotor faults. The need for on-line condition

monitoring of large induction motors has increased because a sudden failure of critical motor can cause great economical losses. Therefore, the main goal of the operator of electrical drives is to reduce the maintenance costs and to prevent unscheduled downtime of these machines (M. E. H. Benbouzid *et al.* 2000).

Failure surveys (Thomson-b *et al.* 2001) have reported that 40% of the motor failures were caused by bearing related failures, 38% by stator winding failures, 10% by rotor related failures and 12% by mixed failures which affect other parts of the machine.

It is possible to detect stator or rotor defects by extracting fault information from line currents, which is so-called, Motor Current Signature Analysis (MCSA) (Thomson-b *et al.* 2001, Henao *et al.* 2005, Joksimovic *et al.* 2001, Nandi *et al.* 1999). This technique is based on the monitoring of stator current spectra. The emergence of spectral components or increase of magnitude of some other components at specific frequencies can be considered as a fault indicator (H. Çalış *et al.* 2008). For this reason, the signal given by stator current sensors must be correctly analysed in both healthy and faulty conditions. It must be recalled that, recently, many new methods are also used for rotor faults detection (A. Widodo *et al.* 2007)

The purposes of this paper is to perform a detailed analytical study for three-phase squirrel cage induction motors, in order to get a comprehensive understanding of the information given by the stator line currents under healthy and faulty states. This study is based on analytical expressions for the stator and the cage rotor MMFs which are derived using the winding function approach. The occurrence of broken rotor bars modifies the equivalent discrete circuit model of the cage rotor. Thus, the influence of this fault can be studied accurately by computing the rotor MMF taking into account the new rotor mesh structure. This is the best method and it is well described in (Henao *et al.* 2005). In this paper, another description is presented to evaluate the effects of broken rotor bars. This way is preferred because it assumes that one broken rotor bar means that one rotor loop is absent. Consequently, the new rotor cage MMF, with broken bar, can be obtained by subtracting rotor MMF induced by the absent loop from the healthy rotor MMF. Moreover, the authors want to illustrate that the phases of rotor cage MMF waves must be expressed in electrical degrees in order to get a logic interpretation of the harmonics which can be appeared in the stator current spectra; otherwise, there will be confusion between the order and the number of pole pairs of these harmonics.

2. Analytical study of the healthy induction motor

2.1. The MMF of symmetrical three-phase stator winding

It is well-known that the stator MMF of each phase is the product of the current and the winding function of this phase (Bossio *et al.* 2004). Thus, for a symmetrical stator winding having three phases: A , B and C , one can write:

$$\begin{cases} F_{sA}(t, \theta) = \sum_n F_{An}^m [\sin(\omega_s t - np\theta) + \sin(\omega_s t + np\theta)] \\ F_{sB}(t, \theta) = \sum_n F_{Bn}^m \left[\sin\left(\omega_s t - \frac{2\pi}{3} - n\left(p\theta - \frac{2\pi}{3}\right)\right) + \sin\left(\omega_s t - \frac{2\pi}{3} + n\left(p\theta - \frac{2\pi}{3}\right)\right) \right] \\ F_{sC}(t, \theta) = \sum_n F_{Cn}^m \left[\sin\left(\omega_s t - \frac{4\pi}{3} - n\left(p\theta - \frac{4\pi}{3}\right)\right) + \sin\left(\omega_s t - \frac{4\pi}{3} + n\left(p\theta - \frac{4\pi}{3}\right)\right) \right] \end{cases} \quad (1)$$

with $n = 2k + 1$ and $k = 0, 1, 2, 3, \dots$

The resulting stator MMF, which is the sum of these three MMFs, is given by:

$$F_s(t, \theta) = \sum_h F_h^m \sin(\omega_s t \pm hp\theta) \quad (2)$$

with, F_h^m is the amplitude of the h^{th} space harmonic and p is the number of pole pairs. It was shown that in the case of balanced three-phase stator windings without neutral connection, all harmonics having triplen pair of poles are cancelled from the resulting stator MMF (Nandi *et al.* 2002). As a result, we must have $h = 6k \pm 1$. However, if the neuter line is connected or there is any unbalanced stator windings, we should have $h = 2k + 1$ with k is an integer. Hence, one can note that beside the fundamental MMF harmonic related to $h = 1$, there exist stator harmonics associated to $h = 5, 7, 11, 13, \dots$ with corresponding $5p, 7p, 11p, \dots$ pair of poles, which are due to the space distribution of the stator windings in slots. By assuming uniform air-gap length, the stator windings will produce air-gap flux density waves with the same waveform (harmonics) as the stator MMF.

2.2. The squirrel cage rotor MMF

A squirrel-cage rotor of N_r bars can be described as N_r identical and equally spaced loops. It is evident, that the h^{th} stator flux density harmonic induces currents in the rotor loops with electrical pulsation of $s_h \omega_s$, where $s_h = 1 - h(1 - s)$ and s is the slip. Thus, the rotor loop currents can be written as:

$$\begin{cases} I_{rh1}(t) = I_{rh}^m \cos(s_h \omega_s t) \\ I_{rh2}(t) = I_{rh}^m \cos\left(s_h \omega_s t - hp \frac{2\pi}{N_r}\right) \\ I_{rh3}(t) = I_{rh}^m \cos\left(s_h \omega_s t - 2hp \frac{2\pi}{N_r}\right) \\ \dots \\ I_{rhN_r}(t) = I_{rh}^m \cos\left(s_h \omega_s t - (N_r - 1)hp \frac{2\pi}{N_r}\right) \end{cases} \quad (3)$$

where I_{rh}^m is the amplitude of the rotor loop currents induced by the h^{th} stator flux density harmonics. Therefore, the rotor loop can be assumed as a one-turn coil ($w_r = 1$) with pitch equal to: $\alpha = 2\pi/N_r$. If the magnetic axes of the rotor loop1 is in the centre of the reference frame fixed to the rotor (Fig. 1); then, the function distribution of this loop can be written as:

$$n_{rd\ loop1}(\theta_r) = \begin{cases} 1 & -\frac{\pi}{N_r} < \theta_r < +\frac{\pi}{N_r} \\ 0 & \text{otherwise} \end{cases} \quad (4)$$

Note that $n_{rd\ loop1}(\theta_r)$ is a periodic function. So, it can be resolved in Fourier series as follows:

$$n_{rd\ loop1}(\theta_r) = \frac{1}{N_r} + \sum_{\eta} \frac{2}{\eta\pi} \sin\left(\eta \frac{\pi}{N_r}\right) \cos(\eta\theta_r) \quad (5)$$

where $\eta = 1, 2, 3, \dots$ is the order of the rotor space harmonics and it must be different from kN_r with k an integer.

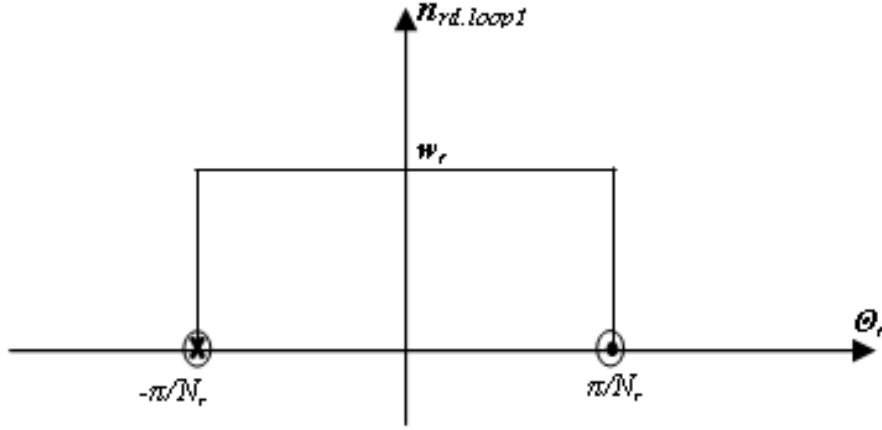


Fig. 1. Distribution function of the rotor loop 1

The winding function, of the first rotor loop, is defined as:

$$N_{rw\ loop1}(\theta_r) = n_{rd\ loop1}(\theta_r) - \langle n_{rd\ loop1}(\theta_r) \rangle \quad (6)$$

where $\langle n_{rd\ loop1}(\theta_r) \rangle = 1/N_r$ is the mean value of the distribution function of the first loop. Since in general case, the induction motors have p pole pairs, the winding function must be express in electrical degrees. Therefore, the winding functions of the rotor loops can be written as follows:

$$\left\{ \begin{array}{l} N_{rw\ loop1}(t, \theta_r) = \sum_{\eta=1}^{\infty} \frac{2}{\eta p \pi} \sin\left(\eta p \frac{\pi}{N_r}\right) \cos(\eta p \theta_r) \\ N_{rw\ loop2}(t, \theta_r) = \sum_{\eta=1}^{\infty} \frac{2}{\eta p \pi} \sin\left(\eta p \frac{\pi}{N_r}\right) \cos\left(\eta p \left(\theta_r - \frac{2\pi}{N_r}\right)\right) \\ N_{rw\ loop3}(t, \theta_r) = \sum_{\eta=1}^{\infty} \frac{2}{\eta p \pi} \sin\left(\eta p \frac{\pi}{N_r}\right) \cos\left(\eta p \left(\theta_r - 2\frac{2\pi}{N_r}\right)\right) \\ \dots\dots\dots \\ N_{rw\ loopN_r}(t, \theta_r) = \sum_{\eta=1}^{\infty} \frac{2}{\eta p \pi} \sin\left(\eta p \frac{\pi}{N_r}\right) \cos\left(\eta p \left(\theta_r - (N_r - 1)\frac{2\pi}{N_r}\right)\right) \end{array} \right. \quad (7)$$

Multiplying (3) by (7) leads to the MMF produced by each rotor loop:

$$\left\{ \begin{array}{l}
 F_{rh\ loop1}(t, \theta_r) = \sum_{\eta=1} F_{rh\eta}^m \left\{ \begin{array}{l} \cos(s_h \omega_s t + \eta p \theta_r) \\ + \cos(s_h \omega_s t - \eta p \theta_r) \end{array} \right\} \\
 F_{rh\ loop2}(t, \theta_r) = \sum_{\eta=1} F_{rh\eta}^m \left\{ \begin{array}{l} \cos\left(s_h \omega_s t + \eta p \theta_r - (\eta + h)p \frac{2\pi}{N_r}\right) \\ + \cos\left(s_h \omega_s t - \eta p \theta_r + (\eta - h)p \frac{2\pi}{N_r}\right) \end{array} \right\} \\
 F_{rh\ loop3}(t, \theta_r) = \sum_{\eta=1} F_{rh\eta}^m \left\{ \begin{array}{l} \cos\left(s_h \omega_s t + \eta p \theta_r - 2(\eta + h)p \frac{2\pi}{N_r}\right) \\ + \cos\left(s_h \omega_s t - \eta p \theta_r + 2(\eta - h)p \frac{2\pi}{N_r}\right) \end{array} \right\} \\
 \dots\dots\dots \\
 F_{rh\ loop N_r}(t, \theta_r) = \sum_{\eta=1} F_{rh\eta}^m \left\{ \begin{array}{l} \cos\left(s_h \omega_s t + \eta p \theta_r - (N_r - 1)(\eta + h)p \frac{2\pi}{N_r}\right) \\ + \cos\left(s_h \omega_s t - \eta p \theta_r + (N_r - 1)(\eta - h)p \frac{2\pi}{N_r}\right) \end{array} \right\}
 \end{array} \right\} \quad (8)$$

Consequently, the resulting MMF of the squirrel rotor cage is the sum of the MMFs of all rotor loops. Thus, we'll have:

$$F_{rh}(t, \theta_r) = \sum_{i=1}^{N_r} \sum_{\eta=1} F_{rh\eta}^m \left\{ \begin{array}{l} \cos\left(s_h \omega_s t + \eta p \theta_r - (i-1)(\eta + h)p \frac{2\pi}{N_r}\right) \\ + \cos\left(s_h \omega_s t - \eta p \theta_r + (i-1)(\eta - h)p \frac{2\pi}{N_r}\right) \end{array} \right\} \quad (9)$$

Equation (9) represents the sum of N_r waves shifted regularly in phase by $(\eta \pm h)2\pi p/N_r$. As a result, this sum is always zero except three cases, when $\eta = \pm h$ as well as for $(\eta + h)p = kN_r$ and $(\eta - h)p = kN_r$. Note that η is a positive integer. Consequently, the cage rotor MMF waves exist only for:

$$\eta = \left\{ \begin{array}{l} |h| \\ \left| \frac{kN_r}{p} \pm h \right| \end{array} \right. \quad (10)$$

It is important to note that if the winding functions of the rotor loops in (7) are expressed in mechanical degrees, we would have: $\eta = |hp|$ and $\eta = |kN_r \pm hp|$ which is the pole pair numbers of space harmonics.

Hence, one can state that each h^{th} stator flux density harmonic produces rotor MMF harmonics with order numbers given by (10). The harmonics having orders equal to $(kN_r/p \pm h)$ are usually called rotor slot harmonics (RSH) which are the consequence of the space distribution of rotor bars. For $k=1$ and $h=1$, we obtain the well-known principle slot harmonics (PSH). So, with respect to the rotor, the squirrel rotor cage MMF can be written as (the general term):

$$\begin{aligned}
F_{rh}(t, \theta_r) = & F_{rh1}^m \cos(s_h \omega_s t \pm hp \theta_r) + \\
& F_{rhSH1}^m \cos \left[s_h \omega_s t + \left(\frac{kN_r}{p} - h \right) p \theta_r \right] + \\
& F_{rhSH2}^m \cos \left[s_h \omega_s t - \left(\frac{kN_r}{p} + h \right) p \theta_r \right]
\end{aligned} \tag{11}$$

To observe (11) from the stator side, we use the transformation given by:

$$\theta_r = \theta - \frac{(1-s)}{p} \omega_s t \tag{12}$$

Thus, the equation (11) can be written as:

$$\begin{aligned}
F_{rh}(t, \theta) = & F_{rh}^m \cos(\omega_s t \pm hp \theta) + \\
& F_{rhSH1}^m \cos \left[\left(1 - \frac{kN_r}{p} (1-s) \right) \omega_s t + \left(\frac{kN_r}{p} - h \right) p \theta \right] + \\
& F_{rhSH2}^m \cos \left[\left(1 + \frac{kN_r}{p} (1-s) \right) \omega_s t - \left(\frac{kN_r}{p} + h \right) p \theta \right]
\end{aligned} \tag{13}$$

By assuming uniform air-gap length, the rotor loops will produce air-gap flux density with the same waveform (harmonics) as the rotor MMF. The rotor flux waves which can induce electromotive forces (EMF) in stator coils are those that have number of pole pairs equal to the pole pair number of the space harmonics of the resulting stator MMF. For example, at healthy state, currents due to the rotor slot harmonic MMF can be flowed in stator windings if only their number of pole pairs

$(kN_r \pm hp)$ belong the set $\{hp\}$. Consequently, for a balanced three-phase stator windings without neutral connection all rotor slot harmonics that have triplen number of pole pairs should not be seen in the stator current spectrum.

3. Current harmonics in case of broken rotor bars

The occurrence of broken rotor bars introduces geometric and magnetic unbalances in the rotor side. Indeed, this fault causes asymmetrical rotor MMF, and this leads to an additional backward and forward rotor flux density waves which induce current components in stator windings with particular frequencies. Since the stator windings structure is not affected by the rotor faults, the stator MMF is still the same as in the healthy conditions while the rotor MMF must be recalculated using the simple approach described above. According to this approach, a rotor squirrel cage with one broken bar will have $(N_r - 1)$ rotor loops instead of N_r . It is so important to note that this approach is less precise, in the sense of evaluating of the magnitudes of induced currents, because, in reality, the current in the broken bar is not zero due to the existence of inter-bar currents. But since our purpose is to evaluate only frequencies of spectral components induced by this fault, the discussed approach is still valid and it can be used. Thus, the new rotor cage MMF with broken rotor bar, can be obtained by subtracting rotor MMF induced by the absent loop from the healthy rotor MMF as follows:

$$F_{rh\eta^*}(t, \theta_r) = F_{rh}(t, \theta_r) - \sum_{i=1}^{nb} F_{rh\eta^*i}(t, \theta_r) \quad (14)$$

with $F_{rh}(t, \theta_r)$ is the resulting rotor MMF of healthy motor given by (11), $F_{rh\eta^*i}(t, \theta_r)$ is the MMF produced by the i^{th} absent rotor loop and nb is the number of broken bars. For example, if the first rotor bar is broken then, the equation (14) can be written as:

$$F_{rh\eta^*}(t, \theta_r) = F_{rh}(t, \theta_r) - F_{rh\eta^*loop1}(t, \theta_r) \quad (15)$$

where:

$$F_{rh\eta^*loop1}(t, \theta_r) = \sum_{\eta^*=1} F_{rh\eta^*}^m \left\{ \begin{array}{l} \underbrace{\cos(s_h \omega_s t - \eta^* p \theta_r)}_{\text{Forward wave}} \\ + \underbrace{\cos(s_h \omega_s t + \eta^* p \theta_r)}_{\text{Backward wave}} \end{array} \right\} \quad (16)$$

with $\eta'' = 1, 2, \dots$ is the order of the space harmonics due to the distribution function of the first rotor loop; it must be different from kN_r , with k an integer. From (16), it is clear that additional backward and forward MMFs, due to the broken bar, exist in the air-gap. It can be seen that they have the same frequency and the identical number of poles. Therefore, (15) can be observed from the stator side using the transformation given by (12), this leads to:

$$\begin{aligned}
F_{r,h,\eta''}(t,\theta) &= F_{rh}^m \cos(\omega_s t \pm hp\theta) \\
&+ F_{rhSH1}^m \cos \left[\left(1 - \frac{kN_r}{p}(1-s) \right) \omega_s t + \left(\frac{kN_r}{p} - h \right) p\theta \right] \\
&+ F_{rhSH2}^m \cos \left[\left(1 + \frac{kN_r}{p}(1-s) \right) \omega_s t - \left(\frac{kN_r}{p} + h \right) p\theta \right] \\
&- \sum_{\eta''=1} F_{rh\eta''}^m \left\{ \underbrace{\cos \left[[1 - (h - \eta'')(1-s)] \omega_s t - \eta'' p\theta \right]}_{\text{Forward wave}} \right. \\
&\quad \left. + \underbrace{\cos \left[[1 - (h + \eta'')(1-s)] \omega_s t + \eta'' p\theta \right]}_{\text{Backward wave}} \right\}
\end{aligned} \tag{17}$$

By assuming uniform air-gap length, the rotor loops will produce rotor air-gap flux density with the same waveform as the rotor MMF (17). Forward and the backward rotor flux density waves can induce EMFs in the stator windings if only their number of pole pair $\eta''p$ belongs to the set $\{hp\}$. Hence, and according to (17), one can state that broken rotor bar faults induce spectral components in stator windings at frequencies given by the following expression:

$$[1 - (h \pm \eta'')(1-s)]f_s \tag{18}$$

Filippetti et al. have reported that the $(1-2s)f_s$ component of the line current interacts with the fundamental air-gap flux to produce torque and speed ripples at $2sf_s$ (Filippetti *et al.* 1998). This phenomenon gives rise to sequence of additional spectral components in the stator currents at frequencies given by:

$$(1 \pm 2ks)f_s, \quad k = 1, 2, 3, \dots \tag{19}$$

Since in practice, the power supply is not purely sinusoidal, currents in phases are also not purely sinusoidal, but contain time harmonics. Taking into account these harmonics, the expressions (18) and (19) can be written, respectively, as follows:

$$[\nu - (h \pm \eta'')(1-s)]f_s \quad (20)$$

$$(\nu \pm 2ks)f_s \quad (21)$$

where $\nu = 1, 3, 5, \dots$ is the order of the time supply harmonics.

Table 1 summarizes the stator current frequency expressions predicted by (20), for $h=1$ and different values of η'' and ν . It is clear that (20) and (21) give the same frequencies. But, it should be known that the components of (20) are due to the presence of space harmonics while those of (21) reflect speed ripples effects brought by the broken rotor bar.

4. Experimental results

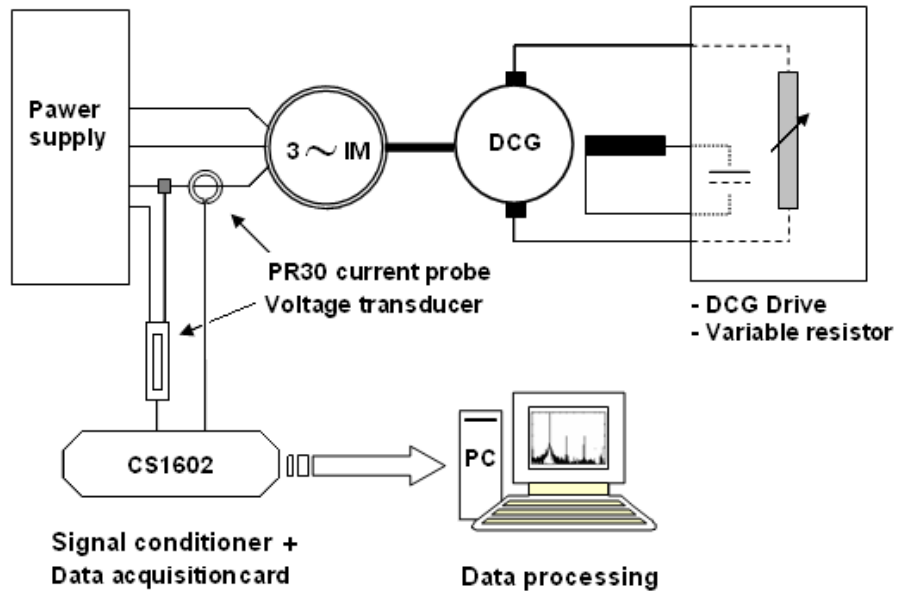


Fig. 2. The experimental setup

The test-motor used in the experimental investigation is a three-phase, 50 Hz, 2-poles, 3kW induction motor and stator windings Y-connected (Fig. 2). Several rotors of identical type could be interchanged. Each of them is a single squirrel cage type with 28 rotor bars. Separately excited DC generator feeding a variable resistor provides a mechanical load. The line current measurements are taken for the motor operating at the nominal rate. Then, the Fast Fourier Transform with a Hanning's window is computed and the power spectrum of the current phase is plotted in the logarithmic magnitude scale and normalized format. The magnitude of the fundamental is assigned to the value of 0 dB. The motor was tested under healthy state and with one broken bar. In order to

observe all the changes brought by the rotor fault, the plots of the stator current spectrums are visualized in three frequencies ranges limited to a bandwidth of 0-100 Hz, 100-400 Hz and 1100-1400 Hz respectively.

Fig.3 – 5 show the three frequency ranges of the line current spectrum for a healthy motor and with one broken bar at the rated speed ($s = 0.055$). It is interesting to note that even healthy motor has some harmonics which coincide with those induced by broken rotor bars given by (20) and (21) but with small magnitudes. They are caused by the inherent rotor asymmetries such as unequal bar resistances that may due to the casting process. Furthermore, one can note the presence of spectral components at 150 Hz, 250 Hz, 350 Hz... with high magnitudes, in both healthy and faulty motor; they represent time supply harmonics characterizing the industrial power distribution system. Previously, it has been demonstrated that for a balanced three-phase squirrel cage induction motor without neutral connection, the spectral components corresponding to $\eta'' = 3, 9, 15...$ should not be present in the current spectrum. Nevertheless, inherent asymmetries in the stator windings as well as a small level of supply voltage unbalance can generate these components which can be easily seen in experimental spectrums. It is so important to know that these inherent asymmetries can not be quantified, since they change notably from a motor to another. Consequently, the magnitudes of the spectral components will also be different from a motor type to another. Concerning the principle slot harmonics (PSH), Fig. 5 shows the existence of the PSH2 at 1373 Hz with -47.4 dB, it has $(N_r + p)$ pole pairs (say 28+1) which belongs to the set $\{(6k \pm 1)p\}$. However, the PSH1 which has $(N_r - p)$ pole pairs (say 28-1) can be clearly seen at 1273 Hz, with very weak magnitude -69 dB, even though theoretically there should be none. This is, most probably, due to the small level of supply voltage unbalance (Ghoggal *et al.* 2006). In addition, it is important to not that time supply harmonics give rise to sequence of additional rotor slot harmonics given by:

$$\left[\nu \pm \frac{kN_r}{p} (1-s) \right] f_s \quad (22)$$

where $\nu = 1, 3, 5, ...$ is the order of the time supply harmonics. For this motor, they appear at 1173 Hz, 973 Hz, 873 Hz... and 1473 Hz, 1573 Hz....

In order to avoid any misinterpretation, all spectral components having magnitudes less than -70 dB are assumed as noise. As can be clearly seen through Fig. 3 and Table 2, the occurrence of one broken rotor bar increases significantly the magnitudes of several sidebands around the fundamental. Furthermore, the Fig. 4 shows, clearly, considerable changes in magnitude for the sidebands around the 3rd, 5th and 7th current time harmonics (Table 4 – 6).

Unfortunately, Fig. 5 does not illustrate important increases in magnitude for the sidebands around the rotor slot harmonics.

In order to more validate this study, the same experimental tests were performed on another three-phase 50 Hz, 4-poles, 28 rotor slots, 1.1kW squirrel cage induction motor with stator windings in Y connection at rated speed ($s = 0.053$).

According to Fig. 6 and Fig. 7, it is obvious that broken rotor bar induces harmonics at the frequencies predicted by (20). But, as can be clearly seen, the spectral components of the 2sd motor (4-poles) have not the same magnitudes as those of the 1st motor (2-poles). This confirms that each motor is a particular case and has a particular stator current spectrum. Consequently, the increases in magnitudes of the spectral components, due to the occurrence of broken rotor bars, can not be efficiently predicted since these magnitudes are influenced by various phenomenons related to the type of motors and to the work conditions surrounding the specific application. However, the detection process can be still possible by analysing both the first and the second frequency ranges and comparing the actual spectrums with the ones references.

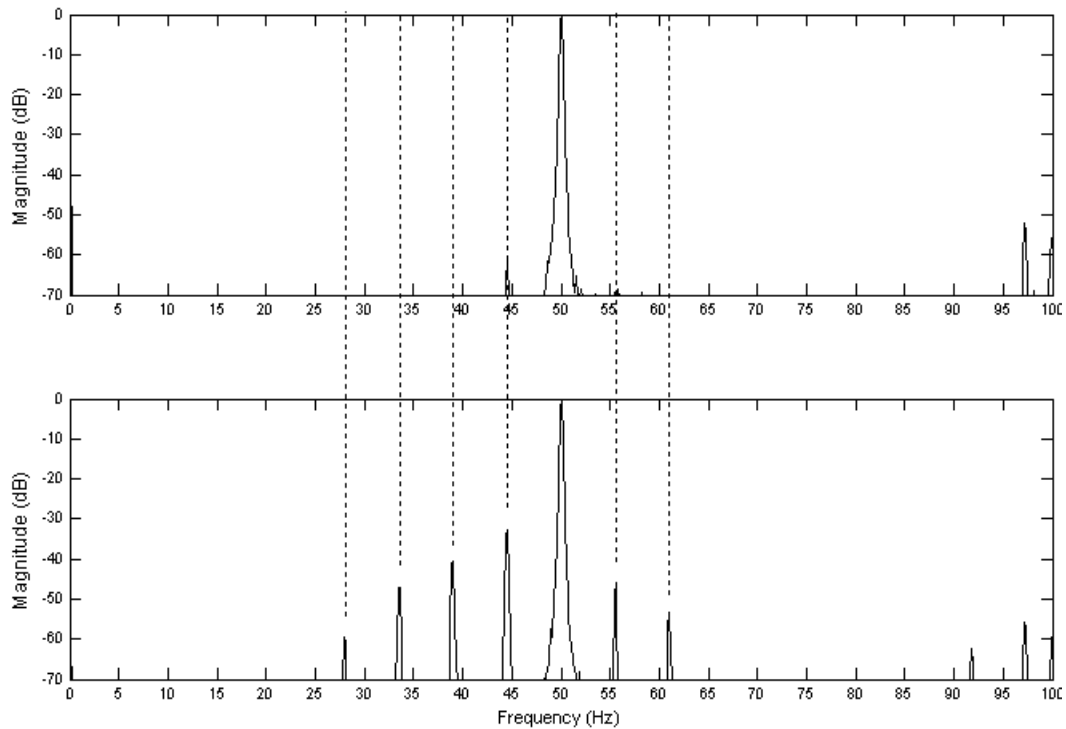


Fig 3. Stator current spectrum at the rated load of a healthy motor (top) and with one broken bar (bottom). First frequency range. (2-poles)

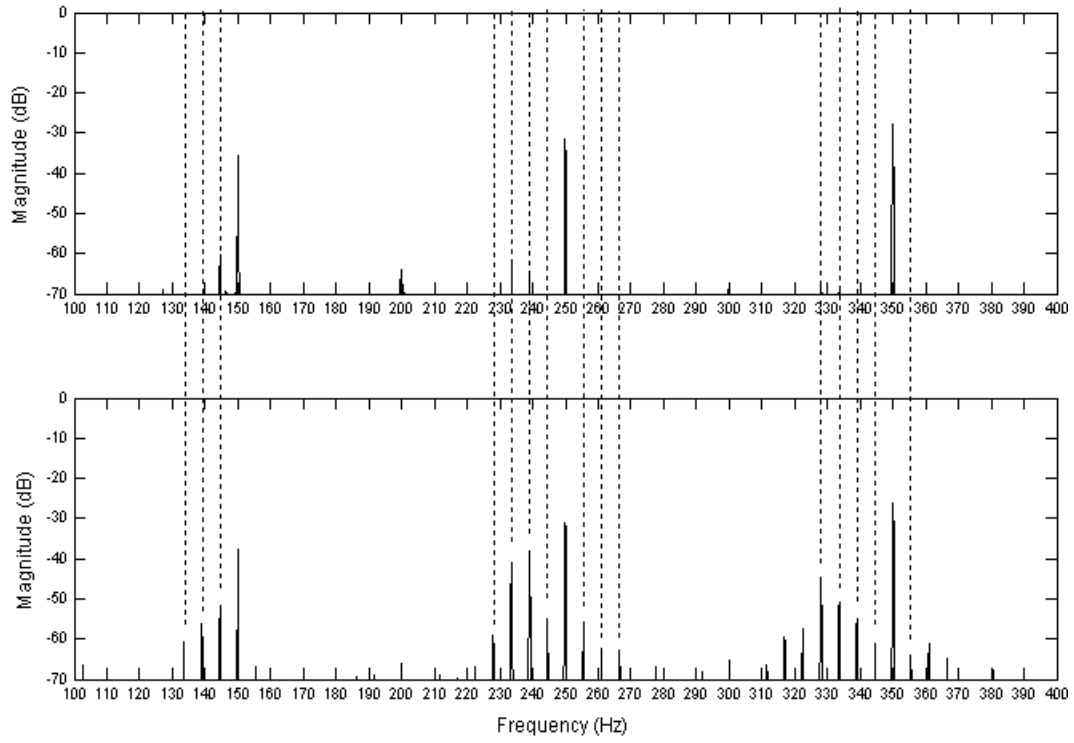


Fig 4. Stator current spectrum at the rated load of a healthy motor (top) and with one broken bar (bottom). Second frequency range. (2-poles)

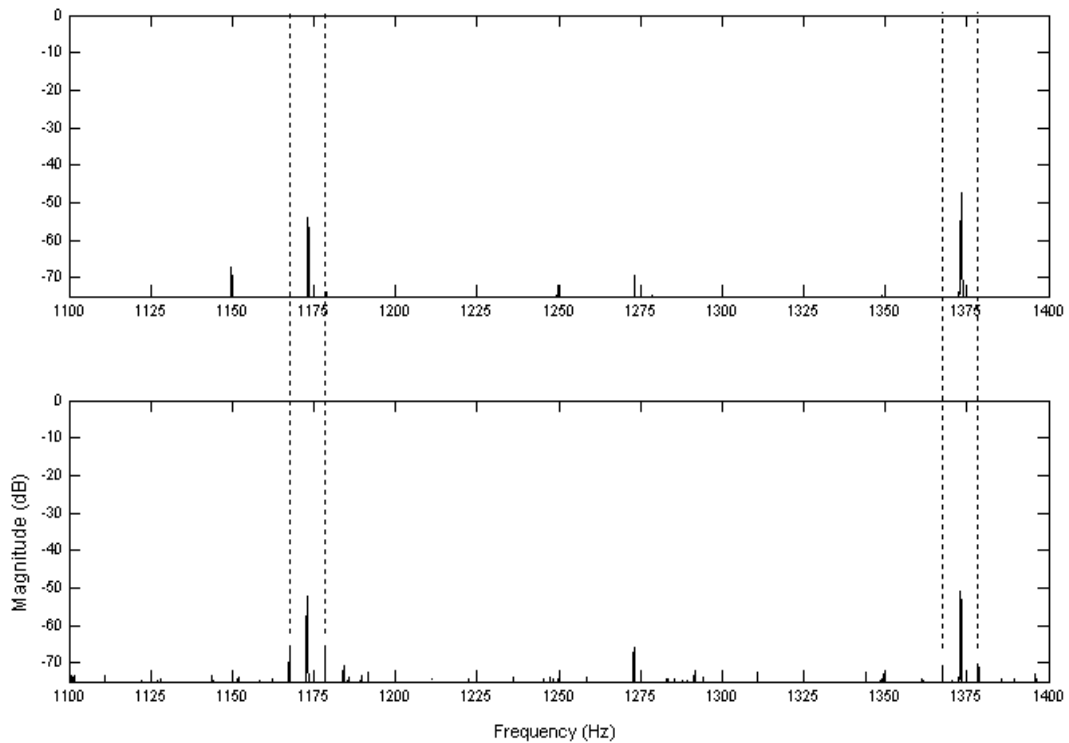


Fig 5. Stator current spectrum at the rated load of a healthy motor (top) and with one broken bar (bottom). Third frequency range. (2-poles)

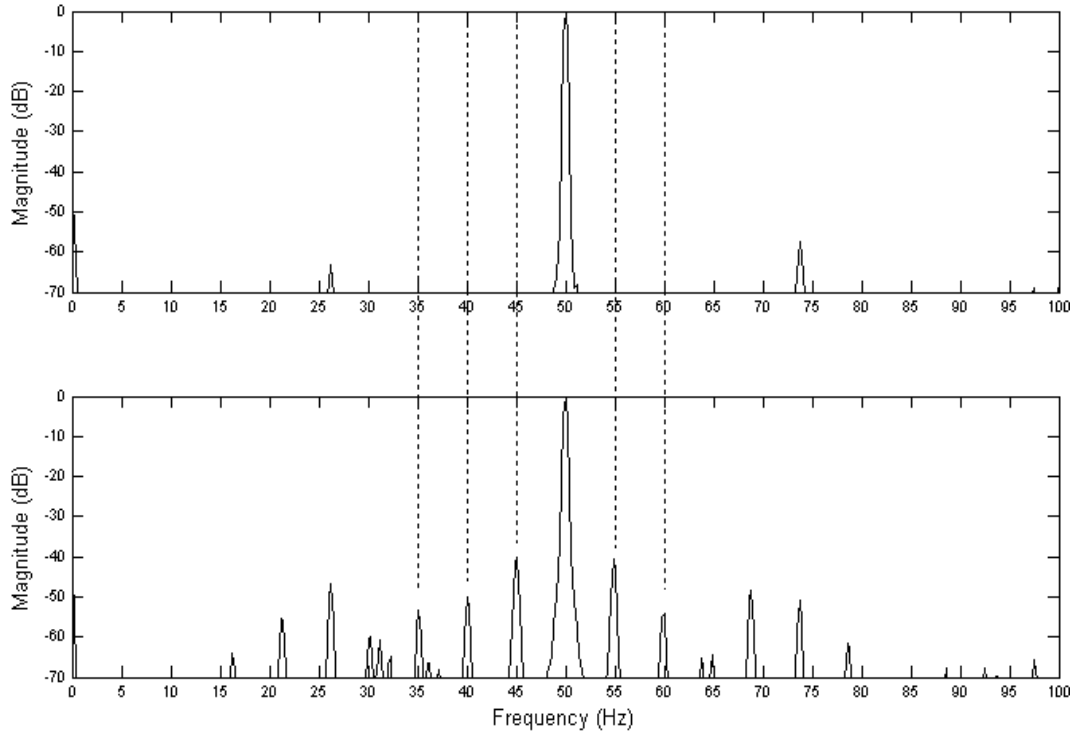


Fig 6. Stator current spectrum at the rated load of a healthy motor (top) and with one broken bar (bottom). First frequency range. (4-poles)

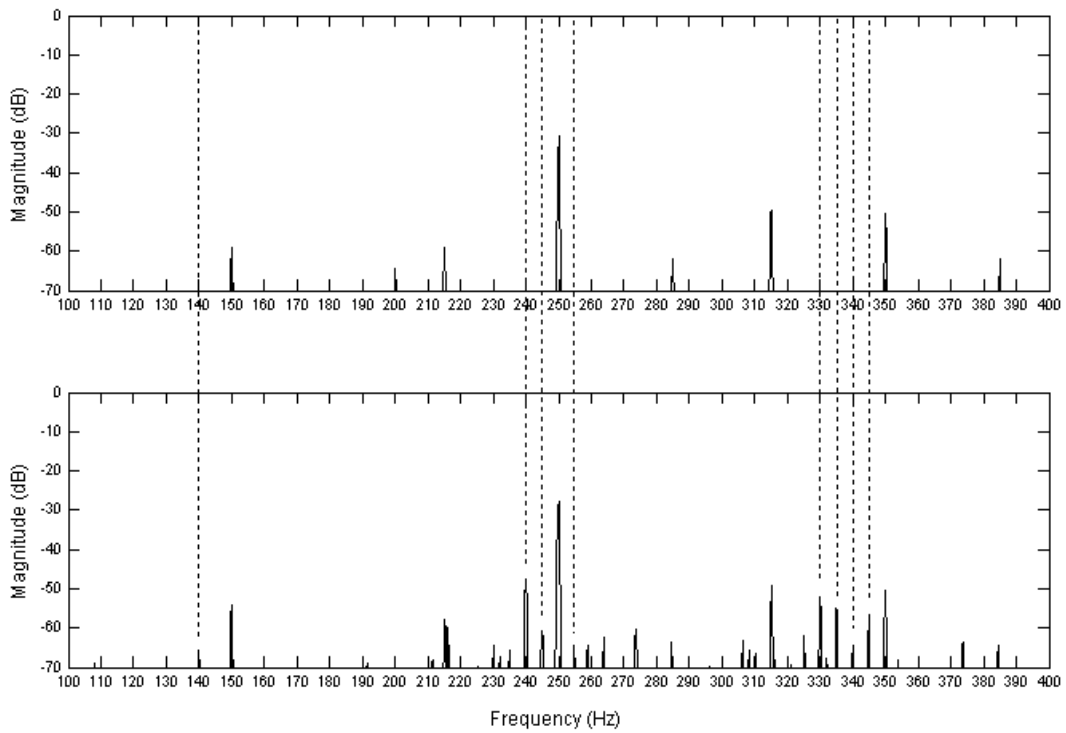


Fig 7. Stator current spectrum at the rated load of a healthy motor (top) and with one broken bar (bottom). Second frequency range. (4-poles)

Table 1. Stator current frequency expressions predicted by (20) for $h = 1$.

η''	Frequency components due to the Forward rotor MMF				Frequency components due to the Backward rotor MMF			
	ν							
	1	3	5	7	1	3	5	7
1	f_s	$3f_s$	$5f_s$	$7f_s$	$(1-2s)f_s$	$(1+2s)f_s$	$(3+2s)f_s$	$(5+2s)f_s$
3	$(3-2s)f_s$	$(5-2s)f_s$	$(7-2s)f_s$	$(9-2s)f_s$	$(3-4s)f_s$	$(1-4s)f_s$	$(1+4s)f_s$	$(3+4s)f_s$
5	$(5-4s)f_s$	$(7-4s)f_s$	$(9-4s)f_s$	$(11-4s)f_s$	$(5-6s)f_s$	$(3-6s)f_s$	$(1-6s)f_s$	$(1+6s)f_s$
7	$(7-6s)f_s$	$(9-6s)f_s$	$(11-6s)f_s$	$(13-6s)f_s$	$(7-8s)f_s$	$(5-8s)f_s$	$(3-8s)f_s$	$(1-8s)f_s$
9	$(9-8s)f_s$	$(11-8s)f_s$	$(13-8s)f_s$	$(15-8s)f_s$	$(9-10s)f_s$	$(7-10s)f_s$	$(5-10s)f_s$	$(3-10s)f_s$
...								

Table 2.

1st frequency range (around the fundamental)					
Expressions	Healthy motor		Faulty motor		Mag. Difference (dB)
	Freq. (Hz)	Mag. (dB)	Freq. (Hz)	Mag. (dB)	
$(1-2s)f_s$	44.5	-61.5	44.5	-32.7	28.8
$(1-4s)f_s$	-	-	39.0	-40.7	29.3
$(1-6s)f_s$	-	-	33.5	-47.0	23.0
$(1+2s)f_s$	55.5	-69.5	55.5	-45.8	23.7
$(1+4s)f_s$	-	-	61.0	-53.4	16.6

Table 3.

2 ^{sd} frequency range (around the third time harmonic)					
Expressions	Healthy motor		Faulty motor		Magn. Difference (dB)
	Freq. (Hz)	Magn. (dB)	Freq. (Hz)	Magn. (dB)	
$(3-2s)f_s$	144.5	-60.4	144.5	-51.7	08.7
$(3-4s)f_s$	-	-	139.0	-56.0	14.0
$(3-6s)f_s$	-	-	133.5	-60.5	09.5
$(3+2s)f_s$	-	-	155.5	-66.6	03.4

Table 4.

2 ^{sd} frequency range (around the fifth time harmonic)					
Expressions	Healthy motor		Faulty motor		Mag. Difference (dB)
	Freq. (Hz)	Mag. (dB)	Freq. (Hz)	Mag. (dB)	
$(5-2s)f_s$	-	-	244.4	-54.8	15.2
$(5-4s)f_s$	239.0	-65.0	239.0	-38.2	26.8
$(5-6s)f_s$	233.6	61.6	233.5	-41.1	20.5
$(5-8s)f_s$	-	-	228.0	-59.1	10.9
$(5+2s)f_s$	-	-	255.6	-55.3	14.7
$(5+4s)f_s$	-	-	261.0	-62.0	08.0

Table 5.

2 ^{sd} frequencies range (around the seventh time harmonic)					
Expressions	Healthy motor		Faulty motor		Mag. Difference (dB)
	Freq. (Hz)	Mag. (dB)	Freq. (Hz)	Mag. (dB)	
$(7 - 2s)f_s$	-	-	344.5	-60.6	09.4
$(7 - 4s)f_s$	-	-	339.0	-54.9	15.1
$(7 - 6s)f_s$	-	-	333.5	-51.0	19.0
$(7 - 8s)f_s$	-	-	328.0	-44.6	25.4
$(7 - 10s)f_s$	-	-	322.5	-57.4	12.6
$(7 + 2s)f_s$	-	-	355.5	-63.9	06.1
$(7 + 4s)f_s$	-	-	361.0	-61.2	08.8

5. Conclusion

In this paper, a detailed analytical study for three-phase squirrel-cage induction motors has been presented. This analysis enabled us to study, with more efficient way, the information given by the stator line currents under healthy and faulty states. It has been proved that all flux density space harmonics from the stator side will be reflected by the rotor at the fundamental frequency and at the rotor slot harmonic frequencies. Consequently, spectral components will appear at these frequencies in the stator current spectrum even in healthy conditions. Also, it was demonstrated that, if rotor cage MMF is expressed in electrical degrees, one can avoid confusion between the order of the rotor space harmonics and their pole pair number.

A fault of broken rotor bars has been studied using a simple approach. It has been mentioned that this approach is limited only to the evaluation of the component frequencies induced by the broken bars fault. In addition, the time supply harmonics were taken into account in order to get the general expressions (20) and (21) which give all the frequencies relating to this rotor fault. The experimental tests which have been carried out on two different motors were found in good agreement with the theoretical analysis.

Acknowledgement

The authors would like to thank Professor Champenois at the LAII laboratory, Poitiers, France, and Professor Hubert Razik at the GREEN laboratory, Nancy, France for their help and support in the experimental tests.

References

1. A. Ghoggal, A. Aboubou, S. E. Zouzou, M. Sahraoui and H. Razik, "Considerations about the modelling and simulation of air-gap eccentricity in induction motors," *IECON'06 Proc. Conf.*, Paris, France, pp. 4987 – 4992, 2006.
2. F. Filippetti, G. Franceschini, C. Tassoni, and P. Vas, "AI Techniques in Induction Machines Diagnosis Including the Speed Ripple Effect," *IEEE Trans. IA*, vol. 34, no.1, pp. 98 – 108, 1998.
3. G. Joksimovic, M. Djurovic and J. Penman, "Cage rotor MMF: Winding Function Approach," *IEE Review in Power Engineering*, pp. 64 – 66, 2001.
4. H. Henao, H. Razik and G. A. Capolino, "Analytical Approach of the Stator Current Frequency Harmonics Computation for Detection of Induction Machine Rotor Faults," *IEEE Trans. IA*, vol. 41, no.3, pp. 801 –807, 2005.
5. M. E. H. Benbouzid, A Review of Induction Motors Signature Analysis as a Medium for Faults Detection, *IEEE Transactions on Industrial Electronics.*, vol. 47, no. 5, 2000, pp. 984-993.
6. G. Bossio, C.D. Angelo, J. Solsona, G. García and M.I. Valla, "A 2-D Model of the induction machine: Extension of the modified winding function approach," *IEEE Trans. Energy Conversion*, Vvol. 19, no. 1, pp. 144-150, Mar. 2004.
7. S. Nandi, R. Bharadwaj, H. A. Toliyat, A. G. Parlos, Study of Three Phase Induction Motors With Incipient Rotor Cage Faults Under Different Supply Conditions, in *Proc. IEEE IAS'99 Annual Meeting Conf.*, vol.3, 1999, pp. 1922-1928.
8. W. T. Thomson-a, On-Line MCSA to Diagnose Shorted Turns in Low Voltage Stator Windings of 3-Phase Induction Motors Prior to Failure, in *Proc. IEMDC*, pp. 1-8, 2001.
9. W. T. Thomson-b and M. Fenger, "Current Signature Analysis to Detect Induction Motor Faults," *IEEE Magazine. IA*, pp. 26 – 34, 2001.
10. H. Çalış, A. Çakır " Experimental study for sensorless broken bar detection in induction motors," *Energy Conversion and Management*, Volume 49, Issue 4, April 2008, Pages 854-862
11. A. Widodo, B. Yang, "Application of nonlinear feature extraction and support vector machines for fault diagnosis of induction motors," *Expert Systems with Applications*, Volume 33, Issue 1, July 2007, Pages 241-250.